Organic & Biomolecular Chemistry

PAPER

View Article Online
View Journal | View Issue

Cite this: *Org. Biomol. Chem.*, 2016, **14**, 3544

Investigation into 9(*S*)-HPODE-derived allene oxide to cyclopentenone cyclization mechanism *via* diradical oxyallyl intermediates†

Sebastien P. Hebert,[a] Jin K. Cha,[a] Alan R. Brash[b] and H. Bernhard Schlegel*[a]

Received 25th January 2016,
Accepted 10th March 2016

DOI: 10.1039/c6ob00204h

www.rsc.org/obc

The cyclopentane core is ubiquitous among a large number of biologically relevant natural products. Cyclopentenones have been shown to be versatile intermediates for the stereoselective preparation of highly substituted cyclopentane derivatives. Allene oxides are oxygenated fatty acids which are involved in the pathways of cyclopentenone biosynthesis in plants and marine invertebrates; however, their cyclization behavior is not well understood. Recent work by Brash and co-workers (*J. Biol. Chem.*, 2013, **288**, 20797) revealed an unusual cyclization property of the 9(*S*)-HPODE-derived allene oxides: the previously unreported 10*Z*-isomer cyclizes to a *cis*-dialkylcyclopentenone in hexane/isopropyl alcohol (100 : 3, v/v), but the known 10*E*-isomer does not yield *cis*-cyclopentenone under the same conditions. The mechanism for cyclization has been investigated for unsubstituted and methyl substituted vinyl allene oxide using a variety of methods including CASSCF, ωB97xD, and CCSD(T) and basis sets up to cc-pVTZ. The lowest energy pathway proceeds *via* homolytic cleavage of the epoxide ring, formation of an oxyallyl diradical, which closes readily to a cyclopropanone intermediate. The cyclopropanone opens to the requisite oxyallyl which closes to the experimentally observed product, *cis*-cyclopentenone. The calculations show that the open shell, diradical pathway is lower in energy than the closed shell reactions of allene oxide to cyclopropanone, and cyclopropanone to cyclopentenone.

Introduction

There is growing interest regarding the mechanistic pathway of allene oxide rearrangement to cyclopentenones, both in experimental biology[1–10] and in computational theory.[11–16] Among the downstream cyclic products arising from biosynthetic pathways containing key allene oxide intermediates are jasmonic acid in plants[17] and clavulones in marine invertebrates.[18] The natural allene oxides are produced by a formal dehydration of unsaturated fatty acid hydroperoxides catalyzed by specialized cytochromes P450 or catalase-related hemoproteins.[19,20] In an aqueous environment the half-life of the allene oxide products is estimated as only 30–40 s at pH 7.4 and 0 °C.[21,22] Nonetheless, rapid extraction and processing under cold conditions has permitted NMR analysis of the methyl ester derivatives.[23] The consistent appearance of the olefinic signals in the proton NMR reveals that, with one exception,[1] the natural allene oxides share a common geometry of the unsaturated epoxyene moiety[23–25] with the double bond impinging on the epoxide in the *E* configuration (Scheme 1).[1,26] The exception was uncovered recently with the discovery that cytochrome P450 CYP74C3 forms two allene

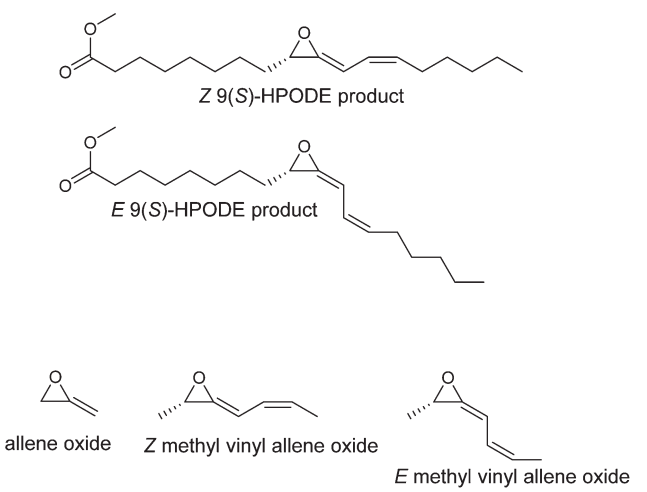

Scheme 1 The allene oxides from 9(*S*)-hydroperoxylinoleic acid and the unsubstituted and substituted allene oxides used in the calculations.

[a]*Department of Chemistry, Wayne State University, Detroit, Michigan 48202, USA. E-mail: hbs@chem.wayne.edu*
[b]*Department of Pharmacology, Vanderbilt University, Nashville, Tennessee 37232, USA*

†Electronic supplementary information (ESI) available: RASSCF orbitals, tables of absolute energies and enthalpies, $\langle S^2 \rangle$ values, and Cartesian coordinates. See DOI: 10.1039/c6ob00204h

oxide stereoisomers from its substrate 9*S*-hydroperoxy-octadeca-10*E*,12*Z*-dienoic acid (9*S*-HPODE), and a mixture of 9,10-epoxy allene oxide methyl esters of the 10*E* and 10*Z* configuration were characterized by NMR (Scheme 1).[1] Significantly, after chromatographic separation of the *E* and *Z* isomers at −15 °C and subsequent exposure to room temperature in the hexane/isopropyl alcohol (100 : 3, v/v) solvent, the *Z* isomer forms cyclopentenone spontaneously, whereas the *E* isomer degrades by reaction with solvent but does not cyclize.[1]

Theoretical studies of the reactions of allene oxides have focused on simplified substituted and unsubstituted allene oxides (Scheme 1).[11–16] Isomerization of the parent allene oxide is believed to proceed *via* ring opening to an oxyallyl intermediate which can close to cyclopropanone.[6,27,28] An experimental investigation into the thermal stereomutation of enantiomerically enriched *trans* di *tert*-butyl cyclopropanone *via* an oxyallyl intermediate found little solvent effect[29,30] ($\Delta G^{\ddagger}$ = 27–29 kcal mol^{-1} for solvents ranging from acetonitrile to isooctane), suggesting the intermediate is a diradical rather than a zwitterion. A recent crystallographic study has provided further evidence of an oxyallyl diradical intermediate.[31] Early calculations on the ring opening of unsubstituted allene oxide at the CASSCF(4,4)/6-31G(d) level of theory likewise found that the oxyallyl intermediate was a diradical and showed that it had a very small barrier for ring closing to cyclopropanone.[29] The CASPT2 calculations yield a free energy of 28 kcal mol^{-1} for the ring opening barrier of cyclopropanone to oxyallyl diradical,[13] in good agreement with the experimental value of 27–29 kcal mol^{-1} for racemization of *trans* di *tert*-butyl cyclopropanone.[30] Later studies showed that spin unrestricted B3LYP density functional and QCISD(T) calculations also gave good values for the relative energies of allene oxide, oxyallyl and cyclopropanone.[13] The singlet and triplet states of oxyallyl diradical have been observed directly by photoelectron spectroscopy and the singlet oxyallyl diradical was found to be 1.3 kcal mol^{-1} lower in energy than the triplet.[28,32] Large basis set CASPT2 and EOM-SP-CCSD(dT) calculations agree with this experimental observation.[10,28,32]

Until recently, studies of the rearrangement of substituted allene oxide to cyclopentenone have assumed *E* stereochemistry for the double bond in allene oxide. Density functional calculations on vinyl substituted *E* allene oxide with the UB3LYP/6-31G(d) level of theory found that the stepwise pathway for the formation of cyclopentenone *via* an oxyallyl intermediate was competitive with the concerted reaction.[11,15] Recent calculations with closed shell density functional theory at the B3LYP/6-311++G(3df,3pd) level found that the stepwise pathway for the vinyl substituted *E* allene oxide *via* a cyclopropanone intermediate to cyclopentenone was lower in energy than the concerted pathway,[14] but this study did not examine the stepwise mechanism for the *Z* isomer. De Lera, Lopez and coworkers have carried out a detailed investigation of methyl substituted vinyl *E* allene oxide[11,16] and *Z* allene oxide[12] using ωB97XD density functional theory with a 6-311++G-(3df,2p) basis set and PCM solvation. The stepwise pathways were found to be comparable in energy for the *E* and *Z* isomers. The concerted pathway is possible only for the *E* isomer but not for the *Z* isomer, and is about 3 kcal mol^{-1} higher in energy than the stepwise path. With spin restricted ωB97XD, the ring opening of allene oxide proceeded directly to vinyl cyclopropanone without a local minimum for oxyallyl. However, with spin unrestricted ωB97XD, an oxyallyl intermediate could be characterized.[16] De Lera and co-workers[12] proposed that cyclopentenone was then formed from vinyl cyclopropanone by a concerted [1,3] sigmatropic rearrangement. The lowest energy pathways led from methyl substituted *Z* vinyl allene oxide to *cis* dimethylcyclopentenone and from the *E* isomer to *trans* dimethylcyclopentenone.

Recent investigation of the reaction of substituted allene oxide used density functional theory and found closed shell pathways for cyclization to cyclopentenone.[12] Because experimental and theoretical studies point to the importance of diradical intermediates, we have re-examined the pathways for the cyclization of methyl vinyl substituted allene oxide to cyclopentenone using theoretical methods such as CASSCF, spin unrestricted CCSD(T) and spin unrestricted density functional theory that are suitable for diradicals. As in previous theoretical studies,[11–16] the present work uses methyl substituted vinyl allene oxide (hereafter simply termed methyl vinyl allene oxide) to model the reactions of the *Z* and *E* 9(*S*)-HPODE products (Scheme 1). These simpler models retain all of the important stereochemical features of the full system. Scheme 2 outlines the possible reaction pathways for the stepwise ring opening of *Z* and *E* methyl vinyl allene oxide to an oxyallyl species, which can adopt a number of conformations/configurations. Oxyallyl can close to vinyl substituted cyclopropanone which, after rotation of the vinyl group, can open to other conformations/configurations of oxyallyl that are able to cyclize to cyclopentenone or dihydrofuran. Cyclopropanone can also rearrange directly to cyclopentenone in a concerted fashion. First, we investigated the reaction of unsubstituted allene oxide to explore the levels of theory needed to study the system, and then we examined the mechanism for methyl vinyl allene oxide.

Method

Calculations were performed with the Gaussian 09 series of programs[33] using complete active space SCF (CASSCF), restricted active space SCF (RASSCF[34]), density functional theory (DFT), coupled cluster (CCSD(T)[35,36]) and Brueckner-Doubles (BD(T)[37]) methods. Spin unrestricted methods were used to calculate diradical states with the DFT, CCSD(T) and BD(T) levels of theory. Optimized gas-phase geometries and vibrational frequencies for the unsubstituted allene oxide pathway were calculated using CASSCF with an active space of 4-electron, 4-orbital (4,4) and the 6-31++G(d,p)[38–41] basis set, and RASSCF with a 20 electron, 19 orbital active space (20,19) and the cc-pVTZ basis set, and DFT with the ωB97xD functional and the cc-pVTZ[42] basis set. For the RASSCF calculations, the RAS1 space consisted of 7 occupied orbitals and

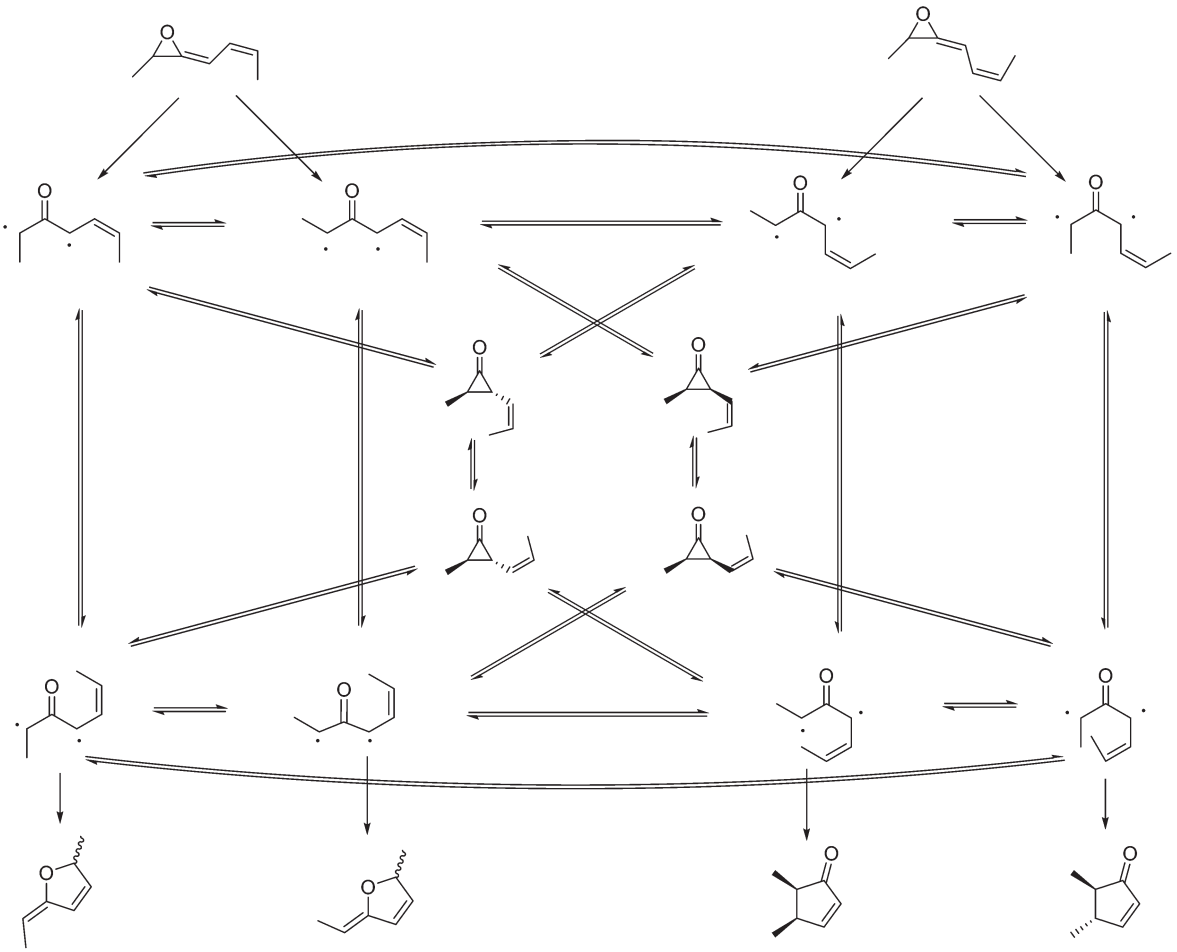

Scheme 2 Pathways for the conversion of *Z*- and *E*-methyl vinyl allene oxide to cyclopentenone and dihydrofuran *via* oxyallyl diradical and cyclopropanone intermediates.

up to 2 holes, the RAS2 space was defined as 6 electrons in 6 orbitals, and the RAS3 space consisted of 6 virtual orbitals with up to 2 electrons. Single point energy calculations were performed with the B3LYP[43–46] and ωB97xD[47] DFT functionals, CASSCF with (4,4), (12,12), and (12,11) active spaces, CASMP2[48] with a (4,4) active space, RASSCF(20,19), and CCSD(T) and BD(T) with cc-pVTZ and aug-cc-pVTZ[49] basis sets using the CASSCF(4,4)/6-311++G(d,p) and UωB97xD/cc-pVTZ gas phase optimized geometries. For the methyl vinyl allene oxide pathways, gas phase optimized geometries, vibrational frequencies and thermal contributions to the enthalpy were calculated using CASSCF(10,8)/6-31++G(d,p) and UωB97xD/cc-pVTZ. Single point energies were calculated with the B3LYP and ωB97XD functionals and with CASSCF and CCSD(T) methods with the cc-pVTZ and aug-cc-pVTZ basis sets using the CASSCF(10,8)/6-31++G(d,p) and UωB97xD/cc-pVTZ optimized geometries. Intrinsic reaction coordinate (IRC) calculations were performed to confirm the nature of the transition states. IRCMax[50] calculations were performed on UωB97xD/cc-pVTZ optimized transition states with UCCSD(T)/cc-pVTZ energies to find an approximate energy of the transition state along the UCCSD(T) surface. For the lowest energy pathways for methyl vinyl allene oxide, the structures were then optimized in solution using the ωB97XD/cc-pVTZ level of theory and the SMD polarizable continuum model[51] for solvation using isopropyl alcohol.

Results and discussion

Unsubstituted allene oxide

To calibrate the computational methods for the study of the conversion of methyl vinyl substituted allene oxide to cyclopentenone, we first consider the potential energy surface for the ring opening of the unsubstituted allene oxide shown in Fig. 1. This system involves an oxyallyl intermediate and has been studied experimentally[28,32] and by a variety of high level theoretical methods.[10,28,32] We have used CASSCF, CASMP2, RASSCF, DFT, CCSD(T), and BD(T) with a number of different basis sets. The (4,4) active space for the CASSCF and CASMP2 calculations of the unsubstituted oxyallyl intermediate includes the carbonyl π and π* orbitals and the in- and out-of-phase p-orbitals having diradical character, as illustrated in Fig. 2. To further probe the effects of dynamic correlation, the

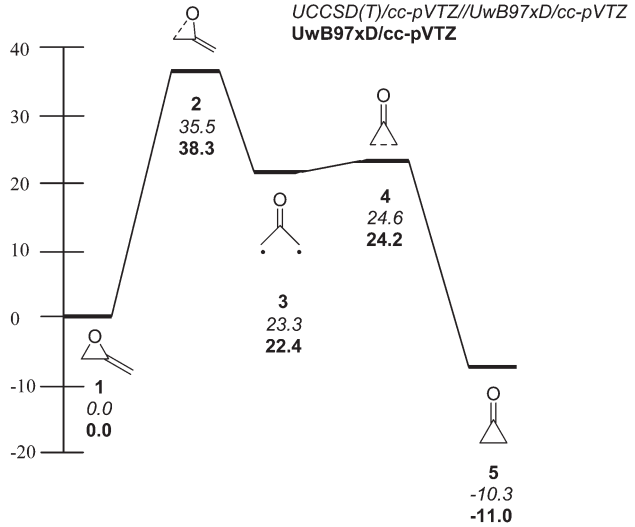

Fig. 1 Cyclization pathway of unsubstituted allene oxide to cyclopropanone *via* oxyallyl intermediate. Energies given in kcal mol^{-1} using cc-pVTZ basis set with UωB97xD/cc-pVTZ optimized geometries.

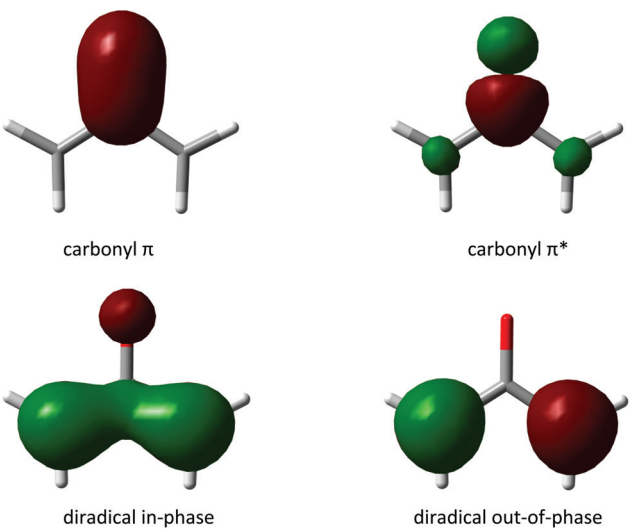

Fig. 2 Orbitals selected for the (4,4) active space used for CASSCF and CASMP2 calculations of unsubstituted allene oxide.

energies were also calculated with CASSCF(12,11) and CASSCF-(12,12). The (12,11) active space included the C–C and C–O sigma bonding and antibonding orbitals associated with the **1** to **3** rearrangement and the (12,12) active space included orbitals that were primarily C–H bonding and antibonding. The orbitals in these two active spaces were combined for the RAS (20,19) calculations. Two holes were allowed in the RAS1 space, which contained all of the C–C, C–H, and C–O bonding orbitals that were not included in the (6,6) RAS2 space, as well the oxygen lone pairs. Two excitations were allowed into the RAS3 space, which contained all relevant antibonding orbitals. The active orbitals are shown in Fig. S1.†

Table 1 Relative energies (in kcal mol^{-1}) of structures along allene oxide cyclization pathway[a]

Method	Basis set	1	2	3	4	5
CASSCF(4,4)[b]	aug-cc-pVDZ	0.0	29.5	10.9	11.0	−12.4
CASSCF(4,4)[b]	cc-pVTZ	0.0	31.5	13.4	13.5	−11.5
CASSCF(4,4)[b]	aug-cc-pvTZ	0.0	31.8	13.3	13.3	−11.3
CASSCF(12,11)[b]	cc-pVTZ	0.0	35.1	14.4	14.9	−12.5
CASSCF(12,12)[b]	cc-pVTZ	0.0	35.0	20.9	20.7	−7.6
RASSCF(20,19)[b]	cc-pVTZ	0.0	36.2	16.5	16.0	−13.1
RASSCF(20,19)[b]	cc-pVDZ	0.0	33.4	15.0	14.6	−14.9
RASSCF(20,19)[c]	cc-pVDZ	0.0	31.4	14.8	14.6[b]	−15.0
RASSCF(20,19)[d]	cc-pVDZ	0.0	30.5	14.2	12.8	−15.1
CASMP2(4,4)[b]	aug-cc-pVTZ	0.0	46.9	28.4	28.1	−5.8
UCCSD[b]	aug-cc-pVTZ	0.0	37.2	21.3	22.3	−10.0
UCCSD(T)[b]	aug-cc-pVTZ	0.0	38.3	24.0	24.8	−9.4
UCCSD(T)[d]	cc-pVTZ	0.0	35.5	23.3	24.6	−10.3
UCCSD(T)[e]	cc-pVTZ		40.1		24.9	
UBD[b]	aug-cc-pVTZ	0.0	37.8	21.4	22.5	−10.1
UBD(T)[b]	aug-cc-pVTZ	0.0	37.0	23.9	24.6	−9.4
UB3LYP[b]	aug-cc-pVTZ	0.0	31.6	19.4	19.9	−9.4
UωB97XD[b]	cc-pVTZ	0.0	37.7	22.5	23.3	−11.0
UωB97XD[b]	aug-cc-pVTZ	0.0	37.1	22.3	23.0	−10.7
UωB97XD[d]	cc-pVTZ	0.0	38.3	22.4	24.2	−11.0
RCCSD[b]	aug-cc-pVTZ	0.0	46.7	33.8	31.6	−10.0
RCCSD(T)[b]	aug-cc-pVTZ	0.0	33.9	25.4	24.2	−9.4
RBD[b]	aug-cc-pVTZ	0.0	48.9	34.1	32.0	−10.1
RBD(T)[b]	aug-cc-pVTZ	0.0	38.0	25.8	24.2	−9.4
RB3LYP[b]	aug-cc-pVTZ	0.0	37.8	30.6	28.0	−9.4
RwB97XD[b]	aug-cc-pVTZ	0.0	46.5	37.4	35.0	−10.7

[a] See Fig. 1 for structure numbers; relative energies without ZPE or thermal corrections (CASSCF(4,4)/6-311++G(d,p) ZPE for **1–5**: 40.2, 37.2, 37.5, 37.5, 40.3 kcal mol^{-1} and ΔH_{0-298} for **1–5**: 2.5, 2.6, 3.2, 2.6, 2.4 kcal mol^{-1}; UωB97XD/cc-pVTZ ZPE for **1–5**: 39.1, 35.6, 36.0, 36.2, 38.4 kcal mol^{-1} and ΔH_{0-298} for **1–5**: 2.4, 2.6, 3.1, 2.5, 2.6 kcal mol^{-1}). [b] CASSCF(4,4)/6-311++G(d,p) gas phase optimized geometry. [c] RASSCF (20,19)/cc-pVDZ gas phase optimized geometry. [d] UωB97XD/cc-pVTZ gas phase optimized geometry. [e] UCCSD(T)/cc-pVTZ IRCMax energies along the UωB97XD/cc-pVTZ IRC.

The CASSCF and DFT calculations indicate that the oxyallyl intermediate and associated transition states have substantial amounts of diradical character. CAS(4,4) calculations have been used in the past to obtain good optimized geometries for these diradicals. Table 1 shows that the various methods yield a wide range of energies for these structures relative to allene oxide. CAS(4,4)/aug-cc-pVTZ//CAS(4,4)/6-311++G(d,p) calculations give 31.8 kcal mol^{-1} for the allene oxide ring opening barrier and 13.3 kcal mol^{-1} for the energy of oxyallyl relative to allene oxide. The CAS(12,11) and CAS(12,12) calculations represent two different active spaces, and increase the barrier by *ca.* 4 kcal mol^{-1} and the oxyallyl energy by 1–7 kcal mol^{-1}, indicating the importance of including additional dynamic correlation. When the two orbital spaces are combined in the RAS(20,19) calculations, the singlet oxyallyl and the ring opening transition state are both 4 kcal mol^{-1} higher than with CAS(4,4) using the same basis set and geometry. Optimization at the RAS(20,19)/cc-pVDZ level of theory lowers the ring opening barrier by 3 kcal mol^{-1} and yields a geometry intermediate between the CAS and DFT optimized geometries. RAS optimization has negligible effect on the other energies. The CASMP2 calculations yield results that are much higher

than our best estimates (see below) and can be dismissed. Density functional and CCSD(T) calculations should provide good estimates of dynamic electron correlation. The ring opening barriers calculated by UωB97xD are in good agreement with the UCCSD(T) values at the same geometry, but the UB3LYP density functional typically yields barriers that are *ca.* 5 kcal mol^{-1} too low.[52] UωB97xD and UCCSD(T) calculations place oxyallyl 22–24 kcal mol^{-1} above allene oxide. The UCCSD(T) ring opening barrier depends on the geometry used for the transition state. By finding a maximum in the UCCSD(T) energy along the UωB97xD reaction path using the IRCMax approach,[50] the ring opening barrier is estimated to be 40 kcal mol^{-1}. In principle, UBD(T) calculations should be even better for these systems than UCCDS(T). The barriers and relative energies change by only 0–1 kcal mol^{-1} comparing UBD(T) and UCCSD(T). Because the CCSD(T) calculations agree very well with BD(T) but are less costly, they are used to explore the reactions of substituted allene oxide. While spin unrestricted calculations are appropriate for diradicals, some caution is necessary because of spin contamination ($<S^2>$ = 0.7–1.0, see Table S3†). The closed shell spin restricted calculations in Table 1 are generally 6–15 kcal mol^{-1} higher than their open shell unrestricted counterparts, indicating they are unsuitable for these systems with diradical character. The notable exceptions are the RCCSD(T) and RBD(T) calculations. The large perturbative triplets corrections bring the ring opening and oxyallyl energies close to the UCCSD(T) and UBD(T) values. However, such large triples contributions should be viewed with caution. While there is considerable variation in the allene oxide ring opening barrier, all of the calculations agree that the barrier for ring closing of oxyallyl to cyclopropanone is less than 2 kcal mol^{-1}.

While singlet oxyallyl diradical is difficult to compute because of issues such as spin contamination and multireference character, an accurate description of triplet oxyallyl diradical should be easy to obtain with single reference spin unrestricted calculations. Table 2 lists the energies of the singlet and triplet oxyallyl diradicals relative to allene oxide for a variety of levels of theory. The UCCSD(T)/aug-cc-pVTZ and UBD(T)/aug-cc-pVTZ energies for triplets should be the most reliable and are used as reference values. The CASSCF(4,4) energies of triplet oxyallyl diradical are 12–13 kcal mol^{-1} lower than the UCCSD(T) energies with the same basis set. This is likely due to the lack of dynamic correlation inherent in the CASSCF method. Use of (12,11) and (12,12) active spaces give energies that are lower than CCSD(T) by 7.9 and 5.5 kcal mol^{-1}, respectively. RASSCF(20,19)/cc-pVTZ single point energies give better agreement with CCSD(T), but are still 4 kcal mol^{-1} too low. The CASMP2 calculations for the triplet are 3–6 kcal mol^{-1} higher than the UCCSD(T) energies. The UB3LYP energies are about 4–5 kcal mol^{-1} lower than UCCSD(T) with the same basis set, but the UωB97XD relative energies of triplet oxyallyl diradical are in good agreement with UCCSD(T). This suggests that the UωB97XD calculations give reliable relative energies for triplet species.

Table 2 Energies (in kcal mol^{-1}) of singlet and triplet spin states of oxyallyl diradical, **3**, relative to allene oxide, **1**

Method[a]	Basis set	Singlet	Triplet	Singlet–triplet[f]
CASSCF(4,4)	6-31G(d)	12.5	7.5	5.0
	6-311++G(d,p)	11.3	7.6	3.7
	cc-pVDZ	11.3	6.6	4.7
	cc-pVTZ	13.4	9.8	3.6
	aug-cc-pVTZ[b]	13.3	10.2	3.1
RASSCF(20,19)	cc-pVDZ[b]	15.0	15.4	−0.4
RASSCF(20,19)	cc-pVDZ[c]	14.2	15.5	−1.3
RASSCF(20,19)	cc-pVDZ	14.8	15.5	−0.7
CASMP2(4,4)	6-31G(d)[b]	26.0	22.4	3.6
	6-311++G(d,p)[b]	24.4	24.1	0.3
	aug-cc-pVTZ[b]	28.4	29.1	−0.7
UCCSD(T)	6-31G(d)[b]	22.3	19.8	2.5
	6-311++G(d,p)[b]	21.4	20.1	1.3
	cc-pVTZ[c]	23.3	22.6	0.7
	cc-pVTZ[b]	24.0	23.3	0.7
	aug-cc-pVTZ[b]	24.0	23.1	0.9
BD(T)	6-31G(d)[b]	22.3	19.7	2.6
	6-311++G(d,p)[b]	21.4	19.9	1.5
	aug-cc-pVTZ[b]	23.9	23.0	0.9
UB3LYP	6-31G(d)	18.8	17.4	1.4
	6-311++G(d,p)	18.1	17.5	0.6
	aug-cc-pVTZ[b]	19.4	18.9	0.5
UωB97XD	6-31G(d)	21.8	19.8	2.0
	6-311++G(d,p)	21.0	19.7	1.3
	cc-pVDZ	21.2	19.3	1.9
	aug-cc-pVTZ[b]	22.3	21.2	1.1
	aug-cc-pVTZ[c]	22.1	21.4	0.7
CASPT2[d]	cc-pVTZ			−0.9
EOM-SF-CCSD(dT)[e]	aug-cc-pVTZ			−1.5
Experiment[d]				−1.3

[a] Optimized with specified method unless otherwise stated; energies are without ZPE or thermal corrections. [b] CASSCF(4,4)/6-311++G(d,p) gas phase optimized geometry. [c] UωB97XD/aug-cc-pVTZ gas phase optimized geometry. [d] Ref. 28. [e] Ref. 10. [f] ZPE(singlet)-ZPE(triplet) = 0.1 kcal mol^{-1} at CASSCF(4,4)/6-311++G(d,p) and UωB97xD/cc-pVTZ.

In a series of experiments using photoelectron spectroscopy, Lineberger and coworkers found that the $^1A_1$ state of oxyallyl diradical was 1.3 kcal mol^{-1} lower than the $^3B_2$ state.[28] The best calculations in the literature (CASPT2 and EOM spin flip CCSD(dT)) find the $^1A_1$ state 0.9 kcal mol^{-1} and 1.5 kcal mol^{-1} lower than $^3B_2$ state.[10,28] With the present CAS(4,4) calculations, the $^1A_1$ state is 3.1 kcal mol^{-1} higher than the $^3B_2$ state. When dynamic correlation is included by CASMP2 and RAS(20,19) at the CAS(4,4) geometries, the singlet state is lower than the triplet state by 0.7 and 0.4 kcal mol^{-1}, respectively. Optimization with RAS(20,19)/cc-pVDZ changes the singlet–triplet gap to 0.7 kcal mol^{-1}. The DFT and CCSD(T) calculations place the $^1A_1$ state 0.5–0.9 kcal mol^{-1} above the $^3B_2$ state. Since the CCSD(T) calculations should be quite reliable for the triplet oxyallyl, this suggests that the CCSD(T) energy of the singlet is about 2 kcal mol^{-1} too high, yielding 22 kcal mol^{-1} as our best estimate for the energy of singlet oxyallyl diradical relative to allene oxide.

The calculations on the unsubstituted allene oxide ring opening indicate CAS(4,4) and UωB97xD yield good geometries, but that large basis sets calculations with UωB97xD and UCCSD(T) are needed for reliable energies. However, prelimi-

Table 3 Comparison of basis sets for the energy of singlet diradical oxyallyl, **3**, relative to allene oxide, **1** (in kcal mol^{-1})[a]

	aug-cc-pVDZ	cc-pVTZ	aug-cc-pVTZ
CASSCF(4,4)	10.9	13.4	13.3
CASMP2(4,4)	21.6	28.4	28.4
UB3LYP	17.6	19.6	19.4
UωB97XD	20.5	22.5	22.3
UCCSD(T)	19.2	24.0	24.0

[a] CASSCF(4,4)/6-311++G(d,p) gas phase optimized geometry.

nary calculations on methyl vinyl allene oxide indicated that CCSD(T) calculations with the aug-cc-pVTZ basis set would be too costly for exploring the reaction mechanism shown in Scheme 2. To obtain a more affordable level of theory, we tried (a) reducing the basis set from aug-cc-pVTZ to aug-cc-pVDZ and (b) removing the extra diffuse function from aug-cc-pVTZ to give cc-pVTZ. Table 3 shows that the aug-cc-pVDZ basis is not suitable since the energies differ by 2–7 kcal mol^{-1} when compared to aug-cc-pVTZ. The energies with the cc-pVTZ basis are within 0.2 kcal mol^{-1} of the larger basis and calculations with this basis are used for the methyl vinyl substituted allene oxide system.

Methyl vinyl allene oxide

The reaction mechanism for the cyclization of methyl vinyl allene oxide shown in Scheme 2. The relative energetics of the numerous pathways were first examined using CASSCF, CCSD(T) and DFT calculations in the gas phase. The geometries and energies were then recalculated in solution using DFT and the SMD polarizable continuum solvation model. The lowest energy profiles for the closed shell and diradical pathways are shown in Fig. 3.

The reaction starts with ring opening to give a substituted oxyallyl intermediate. Since the vinyl group is in conjugation with the oxyallyl group, the π orbitals of the diradical intermediate are delocalized and a larger active space is required for the CASSCF calculations. The 10 electron, 8 orbital active space, shown in Fig. 4, consists of the carbonyl π and π* orbitals, the in- and out-of-phase oxyallyl p-orbitals having diradical character, the vinyl π and π*, and two in-plane orbitals having oxygen lone pair character (LP1 and LP2). Some structures could only be obtained with a smaller 8 electron, 7 orbital active space (omitting LP2). For structures where both the CAS(10,8) and CAS(8,7) calculations converged, the differences in relative energies were below 0.5 kcal mol^{-1}. As Fig. 4 shows, there is strong conjugation between the vinyl group and the diradical, yielding orbitals that resemble allyl radical.

Scheme 3 outlines the ring opening of methyl vinyl substituted allene oxide to oxyallyl and subsequent closing to cyclopropanone. Tables 4 and 5 list the relative enthalpies for various levels of theory at the CAS and ωB97xD optimized geometries (optimization with CCSD(T) is not feasible). For minima, CAS and DFT give very similar geometries, and the UCCSD(T) energies differ by less than 1.5 kcal mol^{-1} between these geometries. For the transition states, the geometries can differ by 0.1 Å for bonds formed or broken, and the UCCSD(T) estimates of the barrier heights can differ by 1–4 kcal mol^{-1} depending on whether the CAS or DFT optimized transition state geometry is used. For the critical allene oxide ring opening steps, more reliable estimates of the UCCSD(T) barriers were obtained by using the IRCMax method to find the maximum in the UCCSD(T) energy along the UωB97xD reaction path.

The *Z*- and *E*-isomers (structures **6** and **7**, resp.) are nearly equal in energy. Each of the isomers can open in two different ways (transition structures **8–11**) yielding four diradical intermediates (**12–15**). Conjugation with the vinyl substituent is expected to stabilize formation of the diradical. The ring opening barriers for the substituted allene oxides **8–11** are 7–10 kcal mol^{-1} lower than the corresponding calculations for the unsubstituted case, **2**. For the CASSCF and spin unrestricted DFT calculations, the epoxide opening transition states for the methyl group rotating away from the oxygen (**9** and **11**) are 2–3 kcal mol^{-1} lower than for the methyl group rotating toward the oxygen (**8** and **10**) due to steric and electronic interactions. The lowest transition state for ring opening of the *Z*-isomer (**9**) is 0.7–1.2 kcal mol^{-1} lower than for the *E*-isomer (**11**) by CAS and DFT. For the UCCSD(T) level of theory, the IRCMax method provides a more reliable estimates of the barriers than using the CAS or DFT optimized geometry, and gives 0.9 kcal mol^{-1} for the difference in the barriers for ring opening of *E*- and *Z*-allene oxide. The CCSD(T) IRCMax and gas phase UωB97XD optimizations result in transition structures that are earlier along the reaction path than the CASSCF and solution UωB97XD optimized geometry, as judged by the C–O distance shown in Scheme 4. Optimization of the transition states with closed shell RωB97XD/aug-cc-pVTZ produced barriers that are about 1–3 kcal mol^{-1} higher than the corresponding open shell structures and have restricted to unrestricted instabilities, indicating that the lowest energy epoxide ring opening transition states have some diradical character.

The ring opening barriers calculated by UωB97XD and UCCSD(T) in the gas phase range from 27 to 36 kcal mol^{-1}, considerably higher than expected for a reaction that occurs rapidly at room temperature. When two explicit molecules of isopropyl alcohol are hydrogen bonded to the oxygen, the barriers were reduced to 17.9 and 18.6 kcal mol^{-1} for the *Z* and *E* isomers, respectively, for the UωB97XD calculations. A more practical method of estimating the solvation energy that can be applied to the entire rearrangement mechanism is the implicit solvation approach which uses a polarizable continuum to represent the solvent. With UωB97XD and SMD implicit solvation calculations using isopropyl alcohol, the barriers were 20.8 and 22.4 kcal mol^{-1} for the *Z* and *E* isomers, respectively. This is commensurate with the rapid rearrangement of *Z*-allene oxide at room temperature observed experimentally.

The results of IRC calculations for the conversion of methyl vinyl allene oxide to cyclopropanone are shown in Fig. 5. The

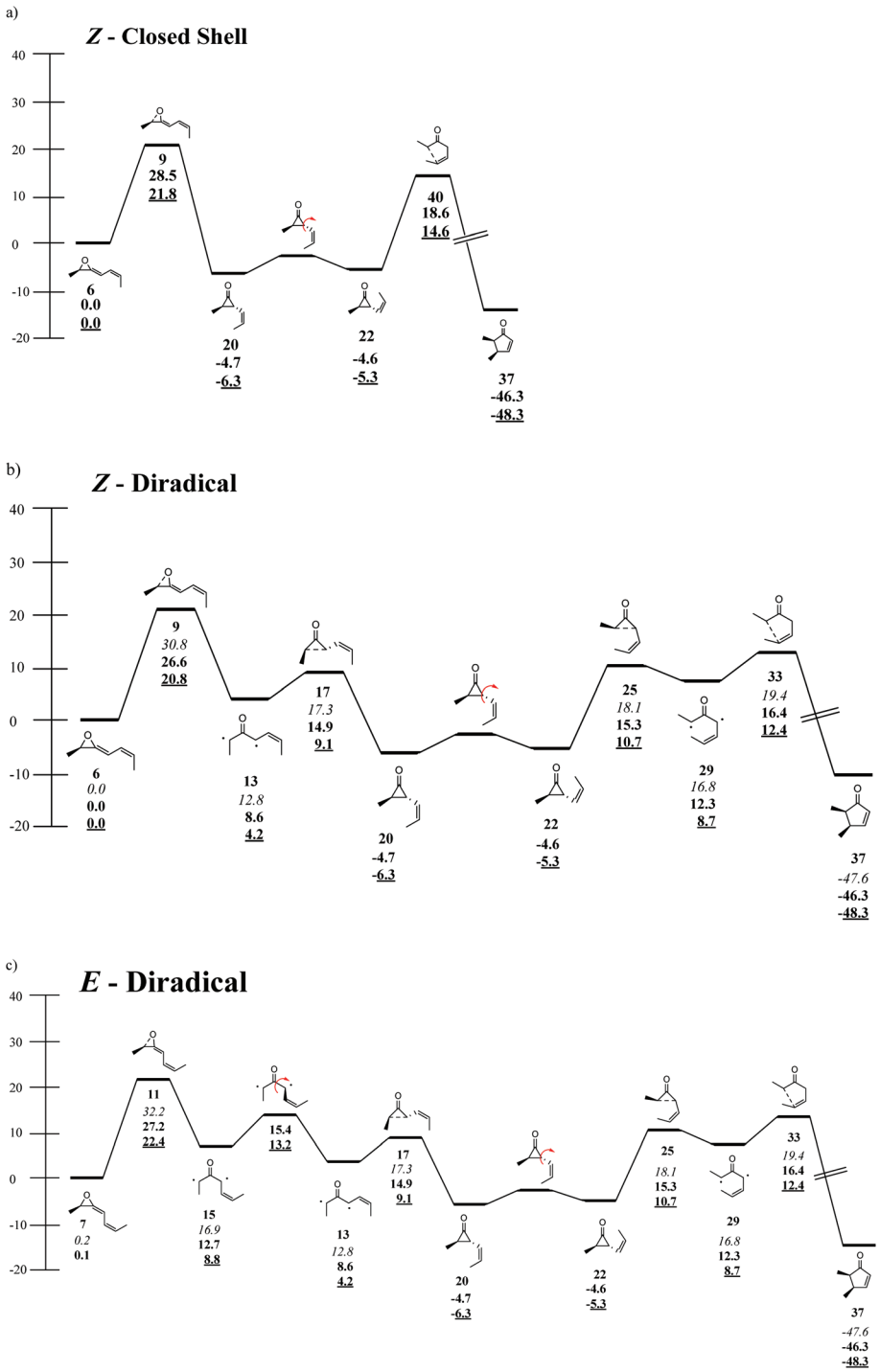

Fig. 3 Lowest enthalpy cyclization pathways of methyl vinyl substituted allene oxide to *cis*-dimethylcyclopentenone: (a) closed shell pathway for *Z*-isomer, (b) open shell diradical pathway for *Z*-isomer, (c) open shell diradical pathway for *E*-isomer in kcal mol^{-1}; CCSD(T)/cc-pVTZ//ωB97xD/cc-pVTZ (italics); ωB97xD/cc-pVTZ gas phase (bold); ωB97xD/cc-pVTZ solution (bold underlined).

closed shell, spin restricted RωB97xD IRC has no oxyallyl minimum, in agreement with the findings of de Lera and co-workers.[12] By contrast, the open shell, spin unrestricted UωB97xD IRCs for both the *Z*- and *E*-isomers show clear minima for the oxyallyl diradicals and barriers of 6–8 kcal mol^{-1} for closure of oxyallyl to cyclopropanone in agreement with the work of Lopez *et al.*[16,53] Since the UωB97xD calculations are in good agreement with higher level calculations for the unsubstituted oxyallyl intermediate and transition states, they should also be reliable for the methyl vinyl oxyallyl intermediates and transition states and give a better representation of the potential energy surface for the reaction than spin

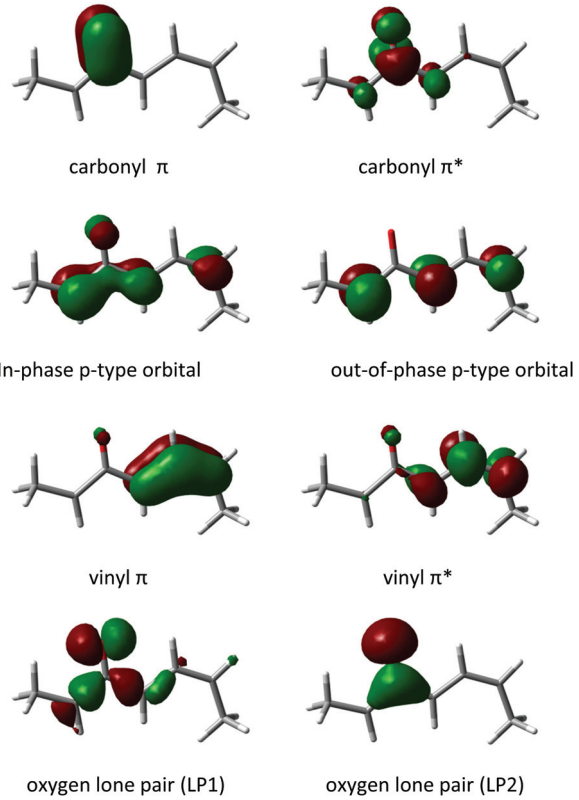

Fig. 4 Orbitals selected for the (10,8) active space for CASSCF and CASMP2 calculations for methyl vinyl allene oxide system. LP2 was dropped for the (8,7) active space calculations.

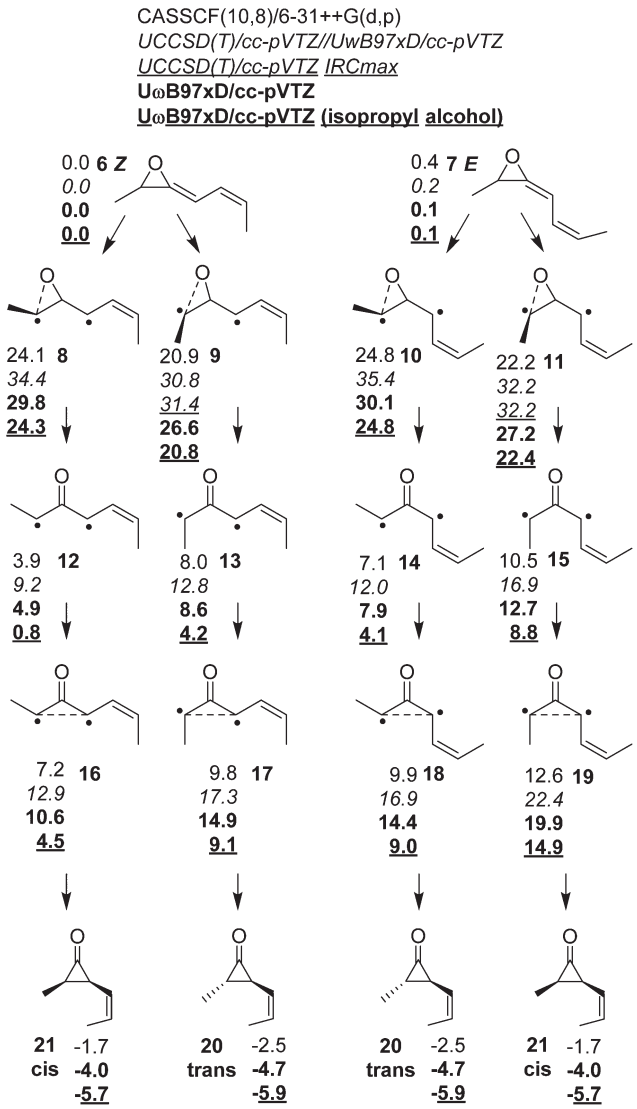

Scheme 3 *Z*- and *E*-methyl vinyl allene oxide (**6** and **7**), transition states for ring epoxide ring opening (**8–11**) to form methyl vinyl oxyallyl diradicals (**12–15**) and transition states for ring closure (**16–19**) to form *trans* and *cis* methyl vinyl cyclopropanones (**20** and **21**). Enthalpies in kcal mol^{-1} calculated at CASSCF(10,8)/6-31++G(d,p) (plain), CCSD(T)/cc-pVTZ//UωB97xD/cc-pVTZ (italics), CCSD(T)/cc-pVTZ IRCMax values (italics, underlined), gas phase UωB97xD/cc-pVTZ (bold) and solution UωB97xD/cc-pVTZ (bold, underlined).

restricted RωB97xD calculations used by de Lera and co-workers.

Relative to allene oxide, the methyl vinyl-substituted oxyallyl intermediates are about 5–10 kcal mol^{-1} more stable than unsubstituted oxyallyl because the diradical is stabilized by strong conjugation with the vinyl group. In **13** and **15**, the CC bond length between the radical center and the vinyl group is nearly equal to the CC bond length within the vinyl group (Scheme 4, *ca.* 1.39 Å in the CAS structures), indicating that it should be regarded as an allyl radical. Structures **13** and **15** are slightly less stable than **12** and **14** because of steric interactions between the hydrogens of the methyl and vinyl groups, as shown in Scheme 4. Solvation stabilizes the singlet diradicals by 3–6 kcal mol^{-1} depending on structure. The triplet methyl vinyl oxyallyl radicals are nearly spin pure but the singlets have S^2 of 0.8–1.0. Similar to the unsubstituted case, the singlet–triplet energy differences for the substituted oxyallyl diradical are small (2 kcal mol^{-1} or less), and removal of the spin contamination should lower the energy by only a small amount.

The oxyallyl diradical readily cyclizes in a disrotatory fashion to produce a cyclopropanone. For the *Z*-isomer, the lowest transition state for allene oxide ring opening yields oxyallyl **13** which cyclizes *via* transition state **17** to *trans*-cyclopropanone, **20.** Correspondingly, ring opening of the *E*-isomer of substituted allene oxide produces oxyallyl **15** which cyclizes *via* **19** to the *cis*-cyclopropanone **21.** The barriers for ring closure of the substituted oxyallyl diradicals are small (4–9 kcal mol^{-1}, Table 5) but are significantly larger than for the unsubstituted case (0–2 kcal mol^{-1}, Table 1). Again, this can be attributed to the stabilizing effect that the vinyl group has on the diradical structure.

Scheme 5 shows the ring opening of the appropriate rotamers of cyclopropanone to configurational isomers of oxyallyl diradical that can close to 5-membered ring products. The barriers for rotation of the vinyl group in the substituted cyclopropanones are small, ~1 kcal mol^{-1} optimized at

Table 4 Enthalpies of methyl vinyl allene oxide and transition states for ring opening (in kcal mol^{-1})[a]

Method	Basis set	6	7	8	9	10	11
CASSCF(10,8)[b]	6-31++G(d,p)	0.0	0.4	24.1	20.9	24.8	22.2
UCCSD[c]	cc-pVTZ	0.0	0.3	36.1	33.1	36.3	33.6
UCCSD(T)[c]	cc-pVTZ	0.0	0.2	34.4	30.8	35.4	32.2
UCCSD(T)[c,d]	cc-pVTZ	0.0			31.4		32.2
UωB97XD[c]	cc-pVTZ	0.0	0.1	29.8	26.6	30.1	27.2
UωB97XD[e]	cc-pVTZ	0.0	0.1	24.3	20.8	24.8	22.4
UωB97XD[f]	cc-pVTZ	0.0			17.9		18.6
RωB97XD[g]	cc-pVTZ	0.0	0.1	31.7	28.5	32.6	31.1
RωB97XD[h]	cc-pVTZ	0.0			21.8		

[a] See Scheme 3 for structure numbers. [b] CASSCF(10,8)/6-31++G(d,p) gas phase optimized geometries, ZPE and ΔH_{0-298}. [c] UωB97XD/cc-pVTZ gas phase optimized geometries, ZPE and ΔH_{0-298}. [d] UCCSD(T)/cc-pVTZ IRCMax energies along the gas phase UωB97XD/cc-pVTZ IRC. [e] UωB97XD/cc-pVTZ solution phase optimized geometries, ZPE and ΔH_{0-298}. [f] UωB97XD/cc-pVTZ geometries, ZPE and ΔH_{0-298} optimized with two isopropyl alcohols hydrogen bonded to the allene oxide. [g] RωB97XD/cc-pVTZ gas phase optimized geometries, ZPE and ΔH_{0-298}. [h] RωB97XD/cc-pVTZ solution phase optimized geometries, ZPE and ΔH_{0-298}.

ωB97XD/cc-pVTZ for both *cis*- and *trans*-cyclopropanone. Since most CC bond rotational barriers for oxyallyl diradical are higher (as discussed below), cyclopropanone acts as a low energy intermediate for the interconversion of the various conformational/configurational isomers of oxyallyl diradical. After rotation of the vinyl group, *cis*- and *trans*-cyclopropanone can each open to two different oxyallyl diradicals, one of which can close to a cyclopentenone, while the other can close to a dihydrofuran. For *trans*-cyclopropanone **22**, the lower energy transition state **25** leads to oxyallyl **29** which has a low barrier (*ca.* 4 kcal mol^{-1}) for closing to *cis*-cyclopentenone **37**. The other cyclopropanone ring opening transition state **24** is *ca.* 3 kcal mol^{-1} higher and leads to **28**, which has a barrier of about 10 kcal mol^{-1} for closing to *E*-dihydrofuran **36**. By contrast, the lower energy transition state for opening *cis*-cyclopropanone **23** leads *via* oxyallyl **30** to *Z*-dihydrofuran **38**, and the higher energy transition state leads *via* **31** to *trans*-cyclopentenone **39**. The lowest energy transition states for oxyallyl intermediates **28–31** closing to a 5-membered ring yields the observed *cis*-cyclopentenone **37**.

In addition to a stepwise diradical pathway, the rearrangement of cyclopropanone to cyclopentenone could occur *via* a closed shell concerted path,[12] as shown in Scheme 6. For *trans*-cyclopropanone, the relative energy of the closed shell concerted transition state optimized at the RωB97XD/aug-cc-pVTZ level of theory is 2 kcal mol^{-1} higher than the barrier for the diradical pathway. Considering that removal of spin contamination is expected to lower the calculated energy of the open shell transition states, diradical ring opening is still favored over closed shell concerted. For *cis*-cyclopropanone, the closed shell transition state **41** is 6 kcal mol^{-1} higher than the diradical transition state **35**. This indicates that the diradical stepwise pathway is preferred over the closed shell concerted pathway for 5-membered ring formation.

Table 5 Relative enthalpies of methyl vinyl oxyallyl, cyclopropanone, and 5-membered ring intermediates and transition states[a]

	CASSCF	UCCSD(T)[d]	ωB97xD[d]	ωB97xD[e]
12	3.9[b]	9.2	4.9	0.8
13	8.0[b]	12.8	8.6	4.2
14	7.1[c]	12.0	7.9	4.1
15	10.5[b]	16.9	12.7	8.8
16	7.2[c]	12.9	10.6	4.5
17	9.8[c]	17.3	14.9	9.1
18	9.9[c]	16.9	14.4	9.0
19	12.6[b]	22.4	19.9	14.9
20	−2.5[c]		−4.7	−6.3
21	−1.7[c]		−4.0	−5.8
22	−2.4[c]		−4.6	−5.3
23	−1.9[c]		−4.4	−5.3
24	14.3[c]	20.2	17.4	12.8
25	11.8[b]	18.1	15.3	10.7
26	11.0[c]	15.3	12.4	7.8
27	14.9[b]	22.0	19.0	14.7
28	13.0[b]	18.1	13.7	10.6
29	11.1[b]	16.8	12.3	8.7
30	9.9[b]	14.2	9.9	7.0
31	13.5[b]	19.7	15.0	12.0
32	24.6[b]		23.6	20.7
33	15.0[b]	19.4	16.4	12.4
34	22.5[b]		20.6	17.7
35	19.5[b]		22.5	19.1
36	−28.2[b]		−29.2	−28.9
37	−44.2[b]	−47.6	−46.3	−48.3
38	−29.7[b]		−30.4	−29.9
39	−46.2[b]		−47.5	−49.5
40			18.6	14.6
41			29.5	25.0

[a] See Schemes 3, 5 and 6 for the structure numbers; enthalpies relative to *Z*-methyl vinyl allene oxide, **6** at the corresponding level of theory. [b] CASSCF(10,8)/6-31++G(d,p) enthalpies using CASSCF(10,8)/6-31++G(d,p) gas phase optimized geometries, ZPE and ΔH_{0-298}. [c] CASSCF(8,7)/6-31++G(d,p) enthalpies using CASSCF(8,7)/6-31++G(d,p) gas phase optimized geometries, ZPE and ΔH_{0-298}. [d] Enthalpies calculated with the cc-pVTZ basis set using ωB97xD/cc-pVTZ gas phase optimized geometries, ZPE and ΔH_{0-298}. [e] Enthalpies calculated with the cc-pVTZ basis set using ωB97xD/cc-pVTZ solution optimized geometries, ZPE and ΔH_{0-298}.

The oxyallyl diradical may be able to convert to different conformers/configurational isomers if the barriers for CC bond rotation are lower than the barriers for cyclization. The possible transitions are shown in Scheme 7 and the barriers are listed in Table 6. The barriers for rotation about the CC bond next to the vinyl group (**12**⇌**30** and **14**⇌**29**) are higher than ring closure to cyclopropanone because of the strong conjugation between the vinyl group and the diradical. The lowest rotational barriers are for **28**⇌**31**, **29**⇌**30**.

Bond rotations in **12–15** can interconvert oxyallyl diradicals originating from *Z*- and *E*-allene oxides, potentially making the initial stereochemistry irrelevant. Conversion from **12–15** to **28–31** is needed for ring closure to the products, and interchange among **28–31** can determine the nature of the final cyclization product. The barriers for converting **12–15** to **28–31** directly by bond rotation are 5–8 kcal mol^{-1} higher than the barriers for ring closure to cyclopropanone. Thus interconversion *via* cyclopropanone is a potential pathway for establishing an equilibrium between the oxyallyl species **12–15** and **28–31**.

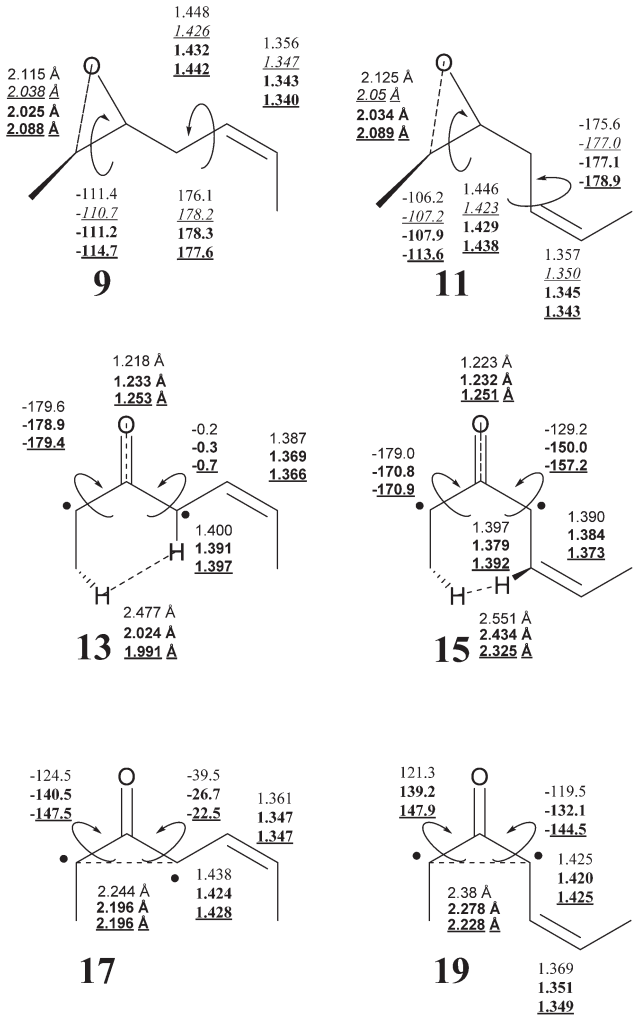

Scheme 4 Comparison of geometries of methyl vinyl oxyallyl intermediates and associated transition states optimized at CASSCF(10,8)/6-31++G(d,p) (plain), CCSD(T) from IRCMax (italics, underlined) levels of theory, gas phase UωB97XD/cc-pVTZ (bold) and solution UωB97XD/cc-pVTZ (bold undelined).

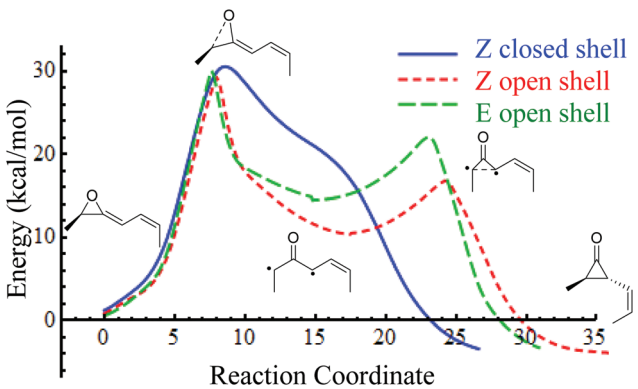

Fig. 5 Intrinsic reaction coordinate for the conversion of methyl vinyl allene oxide to cyclopropanone *via* oxyallyl diradical in the gas phase calculated by RωB97xD/cc-pVTZ for the *Z*-isomer (solid blue line), UωB97xD/cc-pVTZ for the *Z*-isomer (short dashed red line) and the *E*-isomer (long dashed green line).

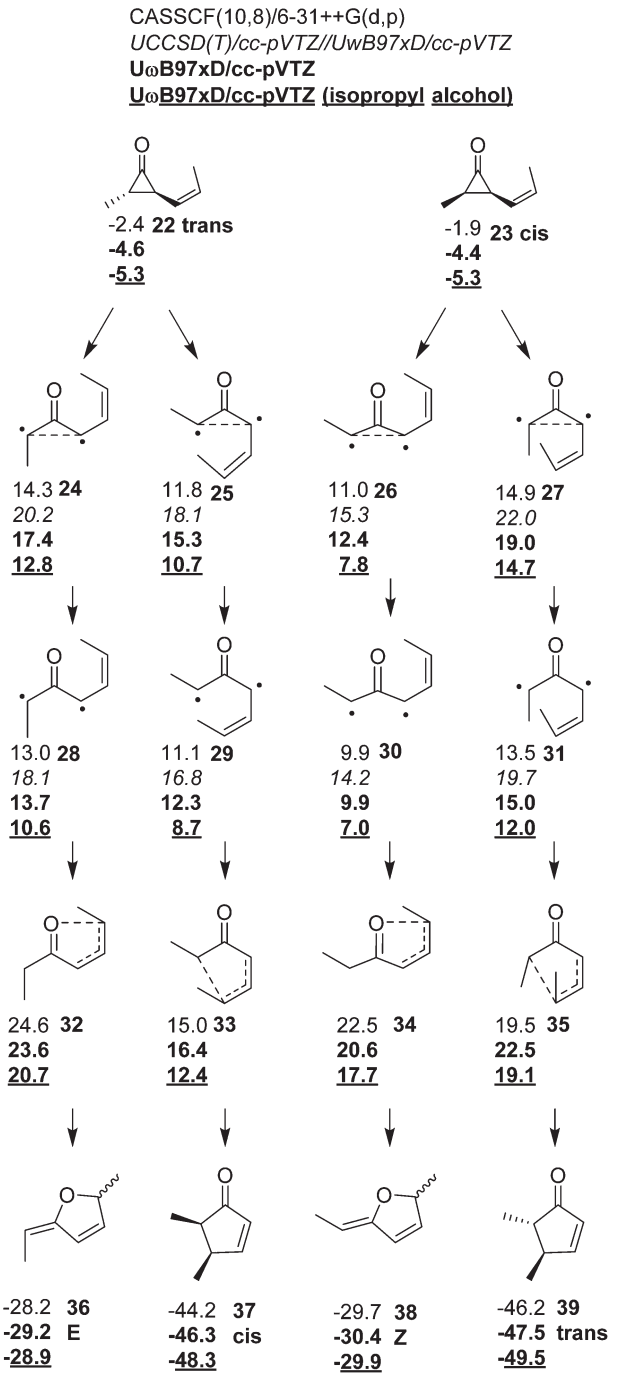

Scheme 5 Conversion of *trans* and *cis* methyl vinyl cyclopropanone (**22** and **23**) to *cis* and *trans* dimethyl cyclopentenone (**37** and **39**) and *E*- and *Z*-dihydrofuran (**36** and **38**) *via* methyl vinyl oxyallyl diradicals (**28–31**). Enthalpies given at CASSCF(10,8)/6-31++G(d,p) (plain), CCSD(T)/cc-pVTZ//UωB97xD/cc-pVTZ (italics), gas phase UωB97xD/cc-pVTZ (bold) and solution UωB97xD/cc-pVTZ (bold underlined).

The nature of the final product would then be determined by the lowest barrier for ring closing to cyclopentenone, dihydrofuran or allene oxide. Since transition state **33** is 4–10 kcal mol^{-1} lower than transition states **32**, **34** and **35** and 10–15 kcal mol^{-1} lower than transition states **8–11**, the final

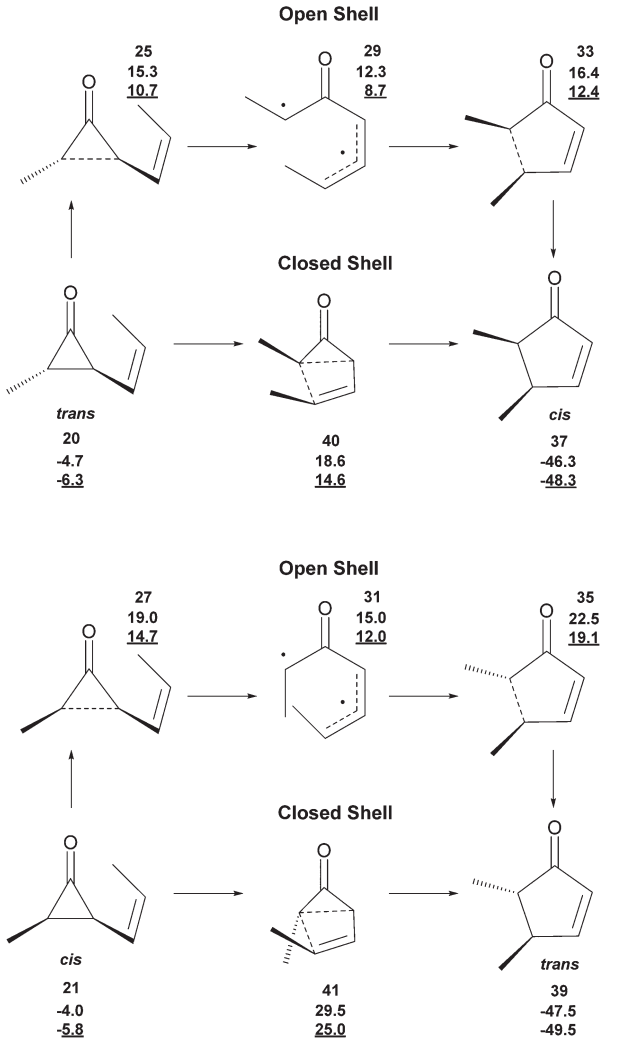

Scheme 6 Enthalpies (in kcal mol^{-1}) for the conversion of *trans* and *cis* methyl vinyl cyclopropanone to cyclopentenone *via* stepwise diradical and closed shell concerted pathways at ωB97XD/aug-cc-pVTZ optimized in the gas phase (bold) and in solution (bold, underlined).

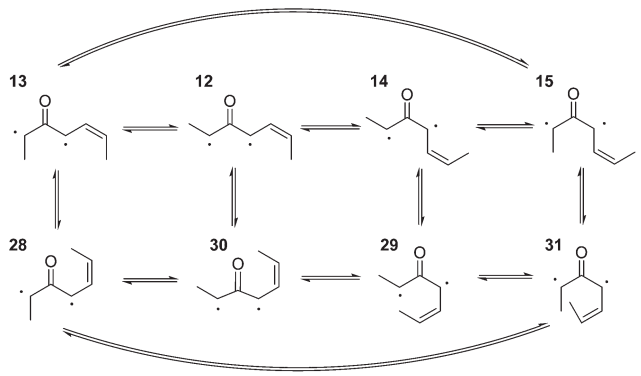

Scheme 7 Interconversion of methyl vinyl oxyallyl diradicals *via* CC bond rotations.

Table 6 Barriers (in kcal mol^{-1}) for CC rotation in oxyallyl diradicals[a]

	UB3LYP	UωB97XD	CASSCF(10,8)
12⇌13	15.2/10.5	14.1/10.4	9.2/4.7
12⇌14	12.4/8.5	10.6/7.4	7.4/4.2
12⇌30	15.8/10.1	14.3/9.2	11.9/6.0
13⇌15	9.1/3.5	7.8/3.2	4.2/1.1
14⇌15	11.3/4.9	10.5/5.4	5.8/1.4
14⇌29	13.4/7.2	11.9/6.8	9.9/5.3
28⇌31	4.1/1.0	2.4/0.8	0.9/0.2
29⇌30	4.1/8.5	3.0/6.2	1.7/3.6

[a] Energy barriers (gas phase, without ZPE or thermal corrections) for forward/reverse reactions calculated with the cc-pVTZ basis set using CASSCF(10,8)/6-31++G(d,p) optimized geometries (transition states not found for **28⇌30**, **29⇌31**, **13⇌28**, **15⇌31**).

product for both *E*- and *Z*-allene oxide cyclization is *cis*-cyclopentenone. The same result can be reached by examining the mechanism one step at a time. Ring opening of *Z*-allene oxide **6** and *E*-allene oxide **7** form different oxyallyl diradicals, **13** and **15** respectively, but only **15** has bond rotation barriers lower than for cyclopropanone ring closing. In particular, the rotation barrier for converting **15** to **13** (3 kcal mol^{-1} for DFT, 1 kcal mol^{-1} for CASSCF) is lower than the barrier for cyclization of **15** *via* **19** to *cis*-cyclopropanone **21** (7–8 kcal mol^{-1} for DFT and 3 kcal mol^{-1} for CASSCF). This would allow ring opening of *E*-allene oxide **7** to form *trans*-cyclopropanone by conversion of **15** to **13**, as shown in Scheme 8, and generate the same *cis*-cyclopentenone product as obtained from *Z*-allene oxide **6**. This pathway is shown in Fig. 3(c) for the rearrangement of *E*-allene oxide to *cis*-cyclopentenone. A similar crossover between the *E*- and *Z*-diradical pathways is possible after cyclopropane ring opening. The barrier for CC bond rotation in **30** to give **29** is about 10 kcal mol^{-1} lower than the barrier for cyclization of **30** to dihydrofuran **38**. Transition state **33** for the conversion of oxyallyl to *cis*-cyclopentanone **37** is lower in energy than the transition states producing other 5-membered ring products (**32**, **34**, **35**) and lower than the transition states for return to allene oxide (**8–11**). Consequently, the various pathways converge to produce the same final product, *cis*-cyclopentanone **37**.

Summary

The energy profiles for stepwise pathways for the conversion of methyl vinyl allene oxide to *cis*-cyclopentenone have been summarized in Fig. 3. The closed shell stepwise pathway for the rearrangement of methyl vinyl allene oxide to *cis*-cyclopentenone *via* cyclopropanone was found to be higher in energy than the corresponding open shell pathways. Open shell calculations indicate that allene oxide opens to oxyallyl diradical which can close to cyclopropanone. Rotation of the vinyl group and opening of cyclopropanone yields a different set of oxyallyl structures. Different conformers/configurational isomers of oxyallyl can also be interconverted by various CC bond rotations. This yields a number of points where *E*- and *Z*-path-

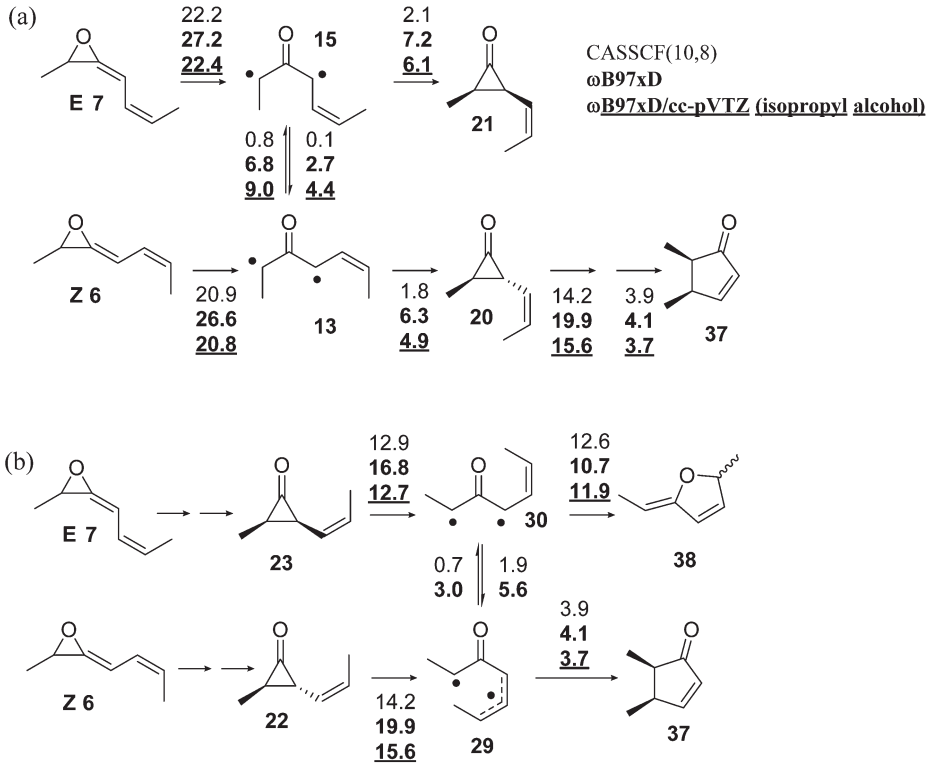

Scheme 8 Convergence of the pathways for cyclization of *E*- and *Z*-methyl vinyl allene oxide. Values indicate the barriers calculated from enthalpies using geometries optimized with CASSCF(10,8)/6-31++G(d,p) (plain) and ωB97XD/cc-pVTZ ind the gas phase (bold) and in solution (bold, underlined).

ways can interconvert (Scheme 8). Appropriate oxyallyl diradicals can close to 5-membered ring products, and the lowest energy transition state is for the formation of *cis*-cyclopentenone. The differences in the barriers for the opening of *Z*- and *E*-methyl vinyl allene oxide to oxyallyl diradical are small and alone do not account for the observed difference in the cyclization behavior of the *Z*- and *E*-isomers. Experimentally, the *cis*-cyclopentenone is found to have an enantiomeric excess of 61 : 39. Since the diradical pathway going through an achiral oxyallyl radical would lead to a racemic mixture of *cis*-cyclopentenone, a small portion of the cyclization has to proceed *via* a pathway that can transfer the chirality of the starting vinyl allene oxide. To explore this alternative, Lopez and coworkers have examined the possible effects of molecular dynamics on the formation of chiral products.[16]

In addition to the formation of cyclopentenone, vinyl substituted allene oxide can react with nucleophiles to produce ring opened products. As a result, the cyclization behavior may depend on the reaction conditions. Grechkin and co-workers were able to observe cyclization of the *E*-isomer to *cis*-cyclopentenone on prolonged storage in hexane.[54] By contrast, in hexane/isopropyl alcohol (100 : 3, v/v) Brash and co-workers found nearly equal amounts of isopropyl alcohol adduct and cyclization product for the *Z*-isomer, but only the isopropyl alcohol adduct for the *E*-isomer.[1] A small increase in the barrier for ring opening can significantly alter the branching ratio when there is competition between cyclization and adduct formation. If the barrier for ring opening of the *E*-isomer is 1–2 kcal mol^{-1} higher than for the *Z*-isomer, and if the barrier for the formation of the isopropyl alcohol adduct is a little lower for the *E*-isomer than the *Z*-isomer, the rate of formation of the adduct will be more favorable than ring opening, and little or no cyclization product will be seen for *E*-isomer. This explanation may reconcile the differing behaviors of cyclization observed by Brash *et al.*[1] and by Grechkin *et al.*[54] The formation of isopropyl alcohol adducts will be the subject of a future study.

Acknowledgements

This work was supported by National Science Foundation grant CHE1464450 (HBS), and in part by NIH grant GM-074888 (to ARB) and a fellowship to SPH from NIGMS/NIH grant R25 GM 058905-17. We thank the Computing Grid at Wayne State University for computer time.

References

1 A. R. Brash, W. E. Boeglin, D. F. Stec, M. Voehler, C. Schneider and J. K. Cha, Isolation and characterization

of two geometric allene oxide isomers synthesized from 9S-hydroperoxylinoleic acid by cytochrome P450 CYP74C3: stereochemical assignment of natural fatty acid allene oxides, *J. Biol. Chem.*, 2013, **288**, 20797–20806.

2 A. Grechkin, Cyclization of natural allene oxide fatty acids. The anchimeric assistance of B,y-double bond besides the oxirane and the reaction mechanism, *Biochim. Biophys. Acta*, 1994, **1213**, 199–206.

3 A. Grechkin and M. Hamberg, Formation of cyclopentanones from all-(E) hydroperoxides of linoleic acid via allene oxides. New insight into the mechanism of cyclization, *FEBS Lett.*, 2000, **466**, 63–66.

4 A. Grechkin, I. R. Chechetkin, L. S. Mukhtarova and M. Hamberg, Role of structure and pH in cyclization of allene oxide fatty acids: Implications for the reaction mechanism, *Chem. Phys. Lipids*, 2002, **120**, 87–99.

5 A. N. Grechkin, L. S. Mukhtarova, L. R. Latypova, Y. Gogolev, Y. Y. Toporkova and M. Hamberg, Tomato CYP74C3 is a multifunctional enzyme not only synthesizing allene oxide but also catalyzing its hydrolysis and cyclization, *ChemBioChem*, 2008, **9**, 2498–2505.

6 A. N. Grechkin, N. V. Lantsova, Y. Y. Toporkova, S. S. Gorina, F. K. Mukhitova and B. I. Khairutdinov, Novel allene oxide synthase products formed via Favorskii-type rearrangement: mechanistic implications for 12-oxo-10,15-phytodienoic acid biosynthesis, *ChemBioChem*, 2011, **12**, 2511–2517.

7 E. Hofmann, P. Zerbe and F. Schaller, The crystal structure of Arabidopsis thaliana allene oxide cyclase: insights into the oxylipin cyclization reaction, *Plant Cell*, 2006, **18**, 3201–3217.

8 P. Neumann, F. Brodhun, K. Sauer, C. Herrfurth, M. Hamberg, J. Brinkmann, J. Scholz, A. Dickmanns, I. Feussner and R. Ficner, Crystal structures of Physcomitrella patens AOC1 and AOC2: insights into the enzyme mechanism and differences in substrate specificity, *Plant Physiol.*, 2012, **160**, 1251–1266.

9 A. R. Brash, S. W. Baertschi and T. M. Harris, Formation of prostaglandin A analogues via an allene oxide, *J. Biol. Chem.*, 1990, **265**, 6705–6712.

10 V. Mozhayskiy, D. J. Goebbert, L. Velarde, A. Sanov and A. I. Krylov, Electronic structure and spectroscopy of oxyallyl: A theoretical study, *J. Phys. Chem. A*, 2010, **114**, 6935–6943.

11 C. Lopez, O. Faza, D. York and A. de Lera, Theoretical study of the vinyl allene oxide to cyclopent-2-en-1-one rearrangement: mechanism, torquoselectivity and solvent effects, *J. Org. Chem.*, 2004, **69**, 3635–3644.

12 A. B. Gonzalez-Perez, A. Grechkin and A. R. de Lera, A unifying mechanism for the rearrangement of vinyl allene oxide geometric isomers to cyclopentenones, *Org. Biomol. Chem.*, 2014, **12**, 7694–7701.

13 B. A. J. Hess, U. Eckart and J. Fabian, Rearrangements of allene oxide, oxyallyl, and cyclopropanone, *J. Am. Chem. Soc.*, 1998, **120**, 12310–12315.

14 G. Audran, P. Brémond, S. R. A. Marque, D. Siri and M. Santelli, Energetics of the biosynthesis of cyclopentenones from unsaturated fatty acids, *Tetrahedron*, 2014, **70**, 8606–8613.

15 B. A. J. Hess, L. Smentek, A. R. Brash and J. K. Cha, Mechanism of the rearrangement of vinyl allene oxide to 2-cyclopenten-1-one, *J. Am. Chem. Soc.*, 1999, **121**, 5603–5604.

16 R. V. Lopez, O. N. Faza and C. S. Lopez, Accounting for diradical character through DFT. The case of vinyl allene oxide Rearrangement, *J. Org. Chem.*, 2015, **80**, 11206–11211.

17 A. Schaller and A. Stintzi, Enzymes in jasmonate biosynthesis - structure, function, regulation, *Phytochemistry*, 2009, **70**, 1532–1538.

18 E. J. Corey, M. d'Alarcao, S. P. T. Matsuda and P. T. J. Lansbury, Intermediacy of 8-(R)-HPETE in the converion of arachidonic acid to pre-clavulone A by Clavularia Viridis. Implications for the biosynthesis of marine prostanoids, *J. Am. Chem. Soc.*, 1987, **109**, 289–290.

19 W. Song, C. D. Funk and A. R. Brash, Molecular cloning of an allene oxide synthase: A cytochrome P450 specialized for the matabolism of fatty acif hydroperoxides, *Proc. Natl. Acad. Sci. U. S. A.*, 1993, **90**, 8519–8523.

20 R. Koljak, O. Boutaud, B. Shieh, N. Samel and A. R. Brash, Identification of a naturally occurring peroxidase-lipoxygenase fusion protein, *Science*, 1997, **277**, 1994–1996.

21 M. Hamberg, Mechanism of corn hydroperoxide isomerase: detection of 12,13(S)-oxido-9(Z),11-octadecadienoic acid, *Biochim. Biophys. Acta*, 1987, **920**, 76–84.

22 M. Hamberg, New cyclopentenone fatty acids formed from linoleic and linolenic acids in potato, *Lipids*, 2000, **35**, 353–363.

23 A. R. Brash, S. W. Baertschi, C. D. Ingram and T. M. Harris, Isolation and characterizaation of natural allene oxides: Unstable intermediates in the metabolism of lipid hydroperoxides, *Biochemistry*, 1988, **85**, 3382–3386.

24 A. R. Brash, Formation of an allene oxide from (8R)-8-hydroperoxyeicosatetraenoic acid in the coral plexaura homomalla, *J. Am. Chem. Soc.*, 1989, **111**, 1891–1892.

25 B. Gao, W. E. Boeglin, Y. Zheng, C. Schneider and A. R. Brash, Evidence for an ionic intermediate in the transformation of fatty acid hydroperoxide by a catalase-related allene oxide synthase from the Cyanobacterium Acaryochloris marina, *J. Biol. Chem.*, 2009, **284**, 22087–22098.

26 N. V. Medvedeva, S. K. Latypov, A. A. Balandina, L. S. Mukhtarova and A. Grechkin, Geometrical configuration of 12,13-epoxyoctadeca-9,11-dienoic acid, a product of the reaction catalyzed by flaxseed allene oxide synthase (CYP74A), *Bioorg. Khim.*, 2005, **31**, 595–596.

27 T. S. Sorensen and F. Sun, An oxyallyl (or oxyallyl-like) geometry is a key structure in the reaction of ketenes and diazonalkanes to form cyclopropanones, *J. Am. Chem. Soc.*, 1997, **119**, 11327–11328.

28 T. Ichino, S. M. Villano, A. J. Gianola, D. J. Goebbert, L. Velarde, A. Sanov, S. J. Blanksby, X. Zhou, D. A. Hrovat, W. T. Borden and W. C. Lineberger, Photoelectron spectro-

scopic study of the oxyallyl diradical, *J. Phys. Chem. A*, 2011, **115**, 1634–1649.
29 D. H. Lim, A. David, W. T. Borden and W. L. Jorgensen, Solvent effects on the ring opening of cyclopropanones to oxyallyls: A combined Ab Initio and Monte Carlo study, *J. Am. Chem. Soc.*, 1994, **116**, 3494–3499.
30 D. B. Sclove, J. F. Pazos, R. L. Camp and F. D. Greene, Thermal reactions of a cyclopropanone. racemization and decarbonylation of trans-2,3-di-tert-butylcyclopropanone, *J. Am. Chem. Soc.*, 1970, **92**, 7488.
31 G. Kuzmanich, F. Spanig, C. K. Tsai, J. M. Um, R. M. Hoekstra, K. N. Houk, D. M. Guldi and M. A. Garcia-Garibay, Oxyallyl exposed: an open-shell singlet with picosecond lifetimes in solution but persistent in crystals of a cyclobutanedione precursor, *J. Am. Chem. Soc.*, 2011, **133**, 2342–2345.
32 T. Ichino, S. M. Villano, A. J. Gianola, D. J. Goebbert, L. Velarde, A. Sanov, S. J. Blanksby, X. Zhou, D. A. Hrovat, W. T. Borden and W. C. Lineberger, The lowest singlet and triplet states of the oxyallyl diradical, *Angew. Chem., Int. Ed.*, 2009, **48**, 8509–8511.
33 M. J. Frisch, G. W. Trucks, H. B. Schlegel, G. E. Scuseria, M. A. Robb, *et al.*, *Gaussian 09 (Revision D. 01)*, Gaussian, Inc., Wallingford, CT, USA, 2009.
34 J. Olsen, B. O. Roos, P. Jorgensen and H. J. A. Jensen, Determinant based configuration interaction algorithms for complete and restricted configuration interaction spaces, *J. Chem. Phys.*, 1988, **89**, 2185–2192.
35 R. J. Bartlett, Many-body perturbation theory and coupled cluster theory for electron correlation in molecules, *Annu. Rev. Phys. Chem.*, 1981, **32**, 359–401.
36 K. Raghavachari, G. W. Trucks, J. A. Pople and M. Head-Gordon, A 5th-order perturbation comparison of electron correlation theories, *Chem. Phys. Lett.*, 1989, **157**, 479–483.
37 N. C. Handy, J. A. Pople, M. Head-Gordon, K. Raghavachari and G. W. Trucks, Size-consistent Brueckner theory limited to double substitutions, *Chem. Phys. Lett.*, 1989, **164**, 185–192.
38 R. Krishnan, J. S. Binkley, R. Seeger and J. A. Pople, Self-consistent molecular orbital methods. XX. A basis set for correlated wave functions, *J. Chem. Phys.*, 1980, **72**, 650–654.
39 T. Clark, J. Chandrasekhar, G. W. Spitznagel and P. V. R. Schleyer, Efficient diffuse function-augmented basis sets for anion calculations. III. The 3-21+G basis set for first-row elements, Li–F, *J. Comput. Chem.*, 1983, **4**, 294–301.
40 R. Ditchfield, W. J. Hehre and J. A. Pople, Self-consistent molecular-orbital methods. IX. An extended gaussian-type basis for molecular-orbital studies of organic molecules, *J. Chem. Phys.*, 1971, **54**, 724–728.
41 W. J. Hehre, R. Ditchfield and J. A. Pople, Self—Consistent Molecular Orbital Methods. XII. Further Extensions of Gaussian—Type Basis Sets for Use in Molecular Orbital Studies of Organic Molecules, *J. Chem. Phys.*, 1972, **56**, 2257–2261.
42 T. H. Dunning, Gaussian basis sets for use in correlated molecular calculations. I. The atoms boron through neon and hydrogen, *J. Chem. Phys.*, 1989, **90**, 1007–1023.
43 A. D. Becke, Density-functional exchange-energy approximation with correct asymptotic-behavior, *Phys. Rev. A*, 1988, **38**, 3098–3100.
44 A. D. Becke, Density-fuctional thermochemistry. 3. The role of exact exchange, *J. Phys. Chem.*, 1993, **98**, 5648–5652.
45 P. J. Stephens, F. J. Devlin, C. F. Chabalowski and M. J. Frisch, *Ab initio* calculations of vibrational absorption and circular-dichroism spectra using density-functional force-fields, *J. Phys. Chem.*, 1994, **98**, 11623–11627.
46 C. T. Lee, W. T. Yang and R. G. Parr, Development of the Colle-Salvetti correlation-energy formula into a functional of the electron-density, *Phys. Rev. B: Condens. Matter*, 1988, **37**, 785–789.
47 J. D. Chai and M. Head-Gordon, Long-range corrected hybrid density functionals with damped atom-atom dispersion corrections, *Phys. Chem. Chem. Phys.*, 2008, **10**, 6615–6620.
48 J. J. W. McDouall, K. Peasley and M. A. Robb, A simple MCSCF perturbation theory: orthogonal valence bond Moller-Plesset 2 (OVB MP2), *Chem. Phys. Lett.*, 1988, **148**, 183–189.
49 R. A. Kendall, T. H. Dunning and R. J. Harrison, Electron affinities of the first-row atoms revisited. Systematic basis sets and wave functions, *J. Chem. Phys.*, 1992, **96**, 6796–6806.
50 D. K. Malick, G. A. Petersson and J. A. Montgomery, Transition states for chemical reactions I. Geometry and classical barrier height, *J. Chem. Phys.*, 1998, **108**, 5704–5713.
51 A. V. Marenich, C. J. Cramer and D. G. Truhlar, Universal solvation model based on solute electron density and on a continuum model of the solvent defined by the bulk dielectric constant and atomic surface tension, *J. Phys. Chem. B*, 2009, **113**, 6378–6396.
52 Y. Zhao, N. Garcia-Gonzalez and D. G. Truhlar, Benchmark database of barrier heights for heavy atom transfer, nucleophilic substitution, association, unimolecular reactions and its use to test theoretical methods, *J. Phys. Chem. A*, 2005, **109**, 2012–2018.
53 R. Kelly, Expression of concern: A unifying mechanism for the rearrangement of vinyl allene oxide geometric isomers to cyclopentenones, *Org. Biomol. Chem.*, 2015, **13**, 11572.
54 N. V. Medvedeva, L. S. Mukhtarova, F. K. Mukhitova, A. A. Balandina, S. K. Latypov and A. N. Grechkin, Cyclization of natural allene oxide in aprotic solvent: formation of the novel oxylipin methyl *cis*-12-oxo-10-phytoenoate, *Chem. Phys. Lipids*, 2007, **148**, 91–96.